Engineered Protein-Iron Oxide Hybrid Biomaterial for MRI-traceable Drug Encapsulation

Lindsay K. Hill[†,‡,§,¶,¤], Dustin Britton[†,¤], Teeba Jihad[†], Kamia Punia, Xuan Xie[†], Erika Delgado-Fukushima[†], Che Fu Liu[†], Orin Mishkit[§,¶], Chengliang Liu[†], Chunhua Hu[∇], Michael Meleties[†], P. Douglas Renfrew[‖], Richard Bonneau[‖,⊥,#], Youssef Z. Wadghiri[§,¶], and Jin Kim Montclare[†,¶,∇,°]*

†. Department of Chemical and Biomolecular Engineering, New York University Tandon School of Engineering, Brooklyn, New York, 11201, USA
‡. Department of Biomedical Engineering, SUNY Downstate Medical Center, Brooklyn, New York, 11203, USA
§.Center for Advanced Imaging Innovation and Research (CAI^{2}R), New York University School of Medicine, New York, New York, 10016, USA
¶.Bernard and Irene Schwartz Center for Biomedical Imaging, Department of Radiology, New York University School of Medicine, New York, New York, 10016, USA
‖. Center for Computational Biology, Flatiron Institute, Simons Foundation, New York, New York, 10010, USA
⊥. Center for Genomics and Systems Biology, New York University, New York, New York, 10003, USA
#. Courant Institute of Mathematical Sciences, Computer Science Department, New York University, New York, New York, 10009, USA
∇. Department of Chemistry, New York University, New York, New York, 10012, USA
°. Department of Biomaterials, New York University College of Dentistry, New York, New York, 10010, USA
¤ Equal contribution
* Corresponding author
Email: Montclare@nyu.edu

SUPPORTING INFORMATION

Determination of Q protein's binding capacity for doxorubicin

The optimal Q protein-to-doxorubicin (Dox) binding ratio was assessed *via* spectrophotometric assay using Q_{WT} protein at 10 µM and 0-100 µM DMSO-dissolved Dox, in 50 mM PB pH 7.4 containing 1% v/v DMSO. The fluorescence intensity of all conditions was assessed spectrophotometrically at 600 nm following overnight (16 hr) binding at 300 rpm and room temperature (**Figure S4**). While an initial plateau in fluorescence intensity occurred at 1:2, the fluorescence was fully saturated at 1:7.5 Q:Dox. Therefore, a 1:5 Q:Dox ratio was considered the near-saturation ratio and used for all Dox binding studies.

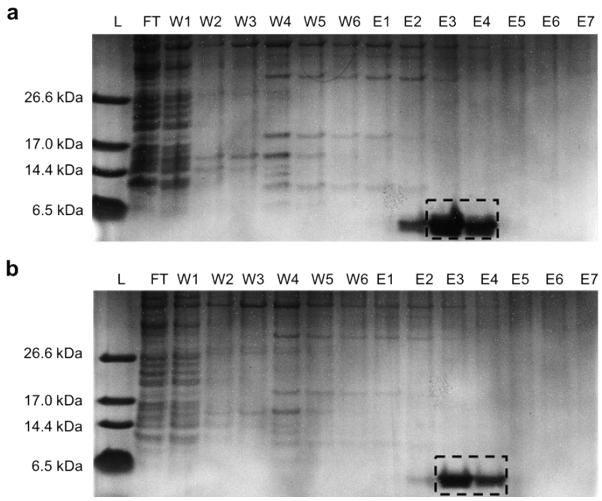

Figure S1. 12% SDS-PAGE of (a) Q_{WT} and (b) Q_{AHA} purified under denaturing conditions *via* immobilized metal affinity chromatography with the following samples: L: ladder, FT: flow through, W1-W3: washes 1-3 using purification buffer with 0 mM imidazole, W4-W6: washes 4-6 using 5 mM imidazole, and E1-E7: elutions 1-7 containing 10, 20, 50, 100, 200, 500, and 500 mM imidazole, respectively. Dashed boxes illustrate elution fractions collected.

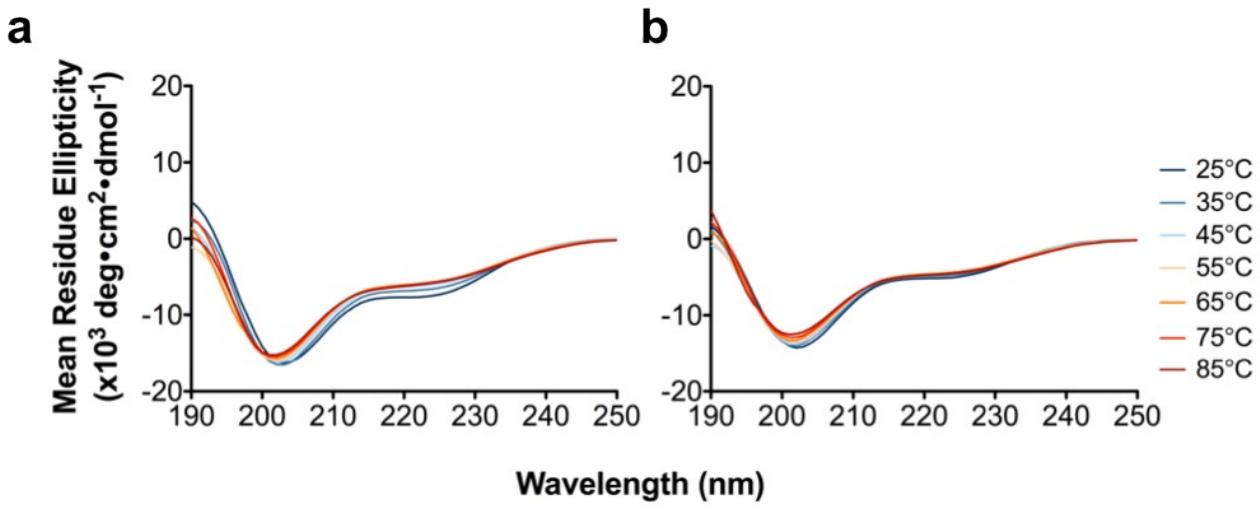

Figure S2. Circular dichroism (CD) of (a) Q_{WT} and (b) Q_{AHA} at pH 4.0 acquired every 10ºC from 25ºC to 85ºC. Data depict the average of three independent trials.

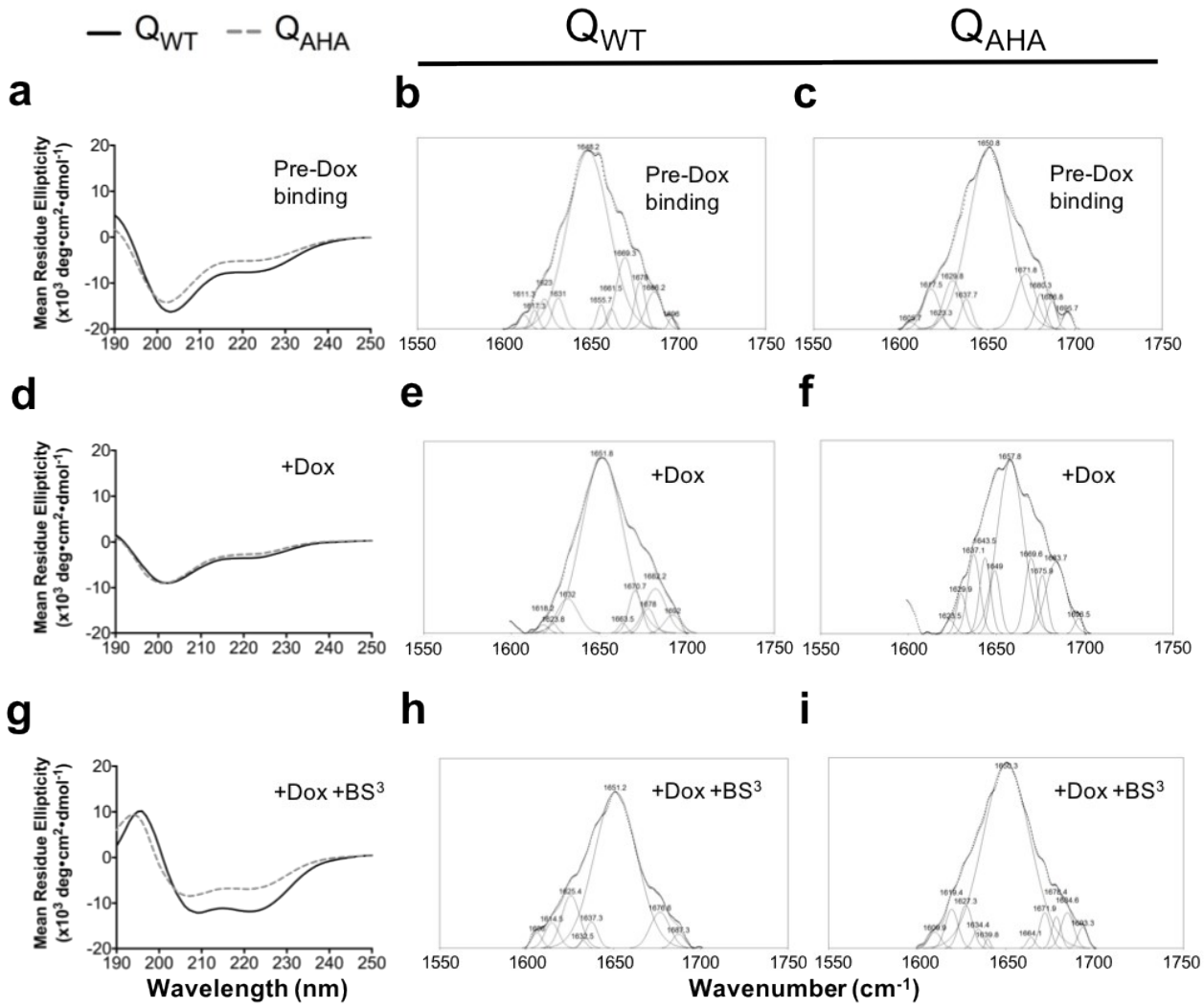

Figure S3. Secondary structure of Q proteins pre- and post-Dox binding and crosslinking. CD wavelength scans and ATR-FTIR spectra acquired for Q_{WT} and Q_{AHA} (a-c) at pH 4.0 prior to Dox binding, (d-f) Dox-bound, and (g-i) Dox-bound and crosslinked. All CD data depict the average of three independent trials and all ATR-FTIR spectra represent two independent trials.

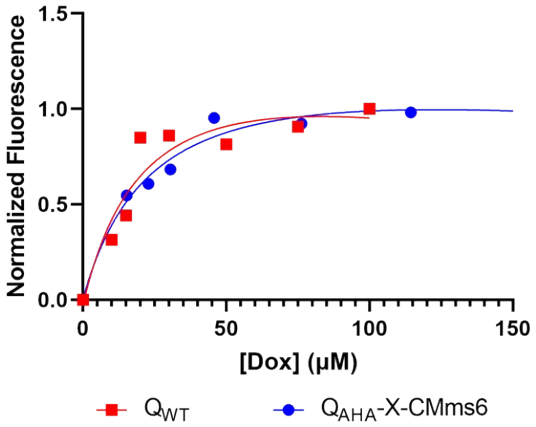

Figure S4. Assessment of Q_{WT}:Dox and Q_{AHA}-X-CMms6:Dox binding ratio. Normalized fluorescence intensity following overnight (16 hr) incubation of 10 μM Q_{WT} protein bound to increasing concentrations of Dox to assess the optimal molar ratio for Dox binding by Q. Binding affinities (Kd) are 24.3 μM Dox and 26.0 μM Dox for Q_{WT} and Q_{AHA}-X-CMms6 respectively indicating saturation at 50 μM or a 1:5 ratio of Dox-to-protein.

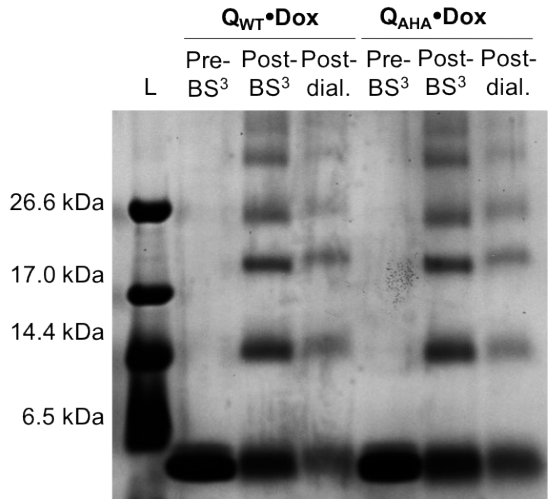

Figure S5. 12% SDS-PAGE including ladder (L) and Dox-bound Q_{WT} and Q_{AHA} mesofibers (Q_{WT}•Dox and Q_{AHA}•Dox) pre- and post-BS^3 chemical crosslinking and following subsequent dialysis.

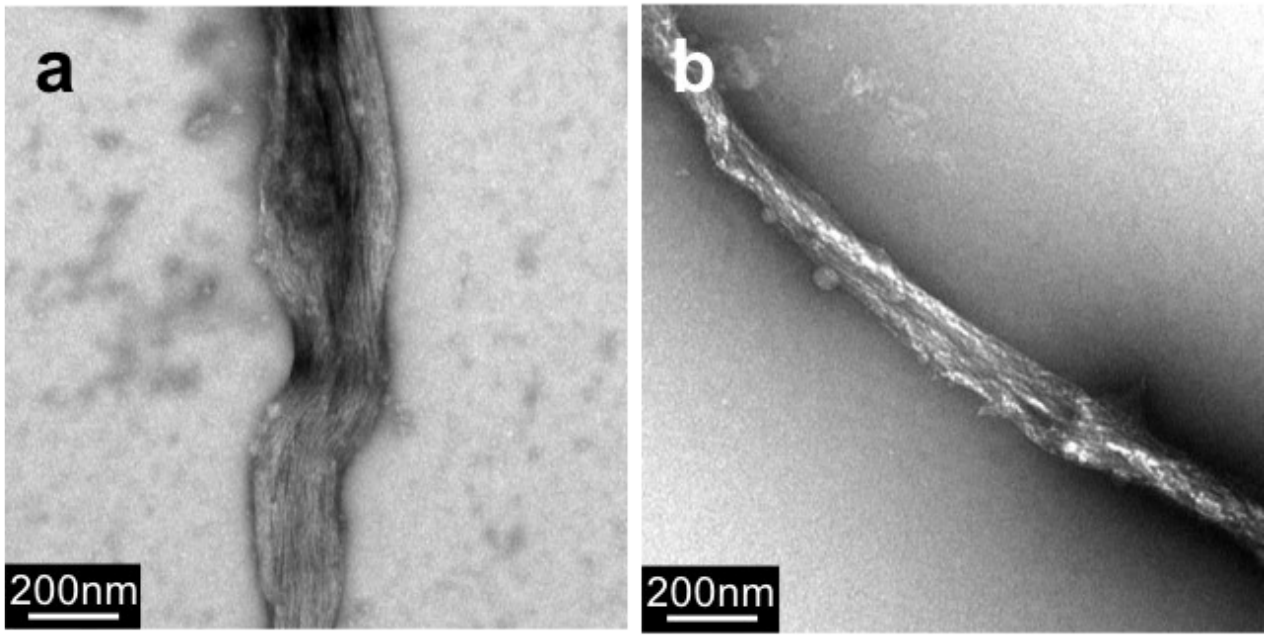

Figure S6. Fiber maintenance under Dox binding conditions in the absence of Dox. Uranyl-acetate-stained TEM following overnight incubation in 50 mM PB pH 7.4 + 1% DMSO of (a) Q_{WT} and (b) Q_{AHA} to confirm nanofiber assembly is maintained under binding conditions in the absence of Dox.

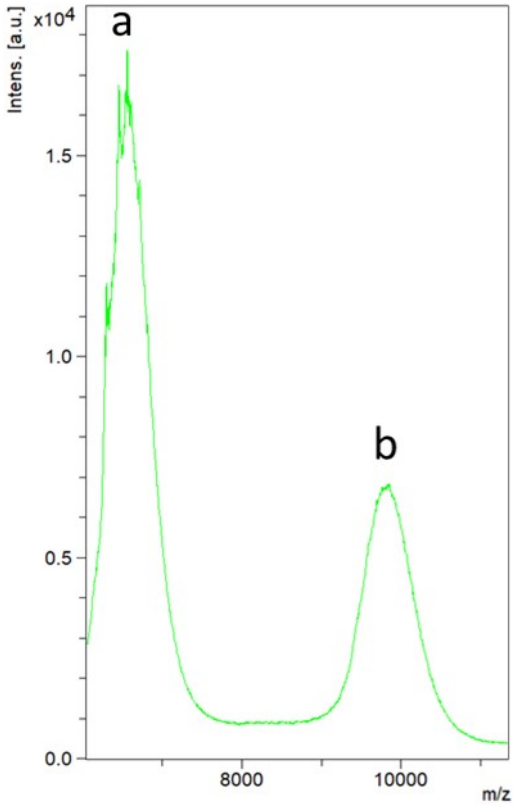

Figure S7. MALDI-TOF spectra after crosslinking of Q_{AHA} and clicking to CMms6 and before dialysis showing a m/z difference corresponding to 2.9 kDa. **a.** Unreacted Q_{AHA} 6.4 kDa. **b)** Q_{AHA} reacted with one CMms6 peptide

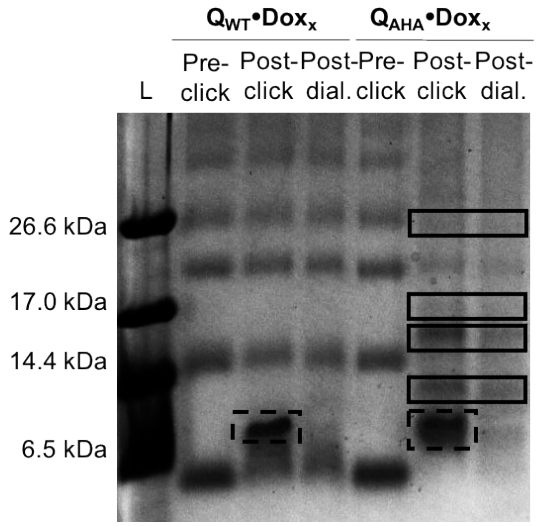

Figure S8. SDS-PAGE assessment of azide-alkyne cycloaddition reaction. 12% SDS-PAGE including ladder (L) and crosslinked Q_{WT} and Q_{AHA} mesofibers (Q_{WT}•Dox_x and Q_{AHA}•Dox_x) pre and post-copper-catalyzed azide-alkyne cycloaddition reaction with alkyne-bearing CMms6 peptide and following subsequent dialysis. Unreacted prg-CMms6 is shown with dashed boxes while solid boxes highlight the clicked product, dubbed Q_{AHA}-X-CMms6.

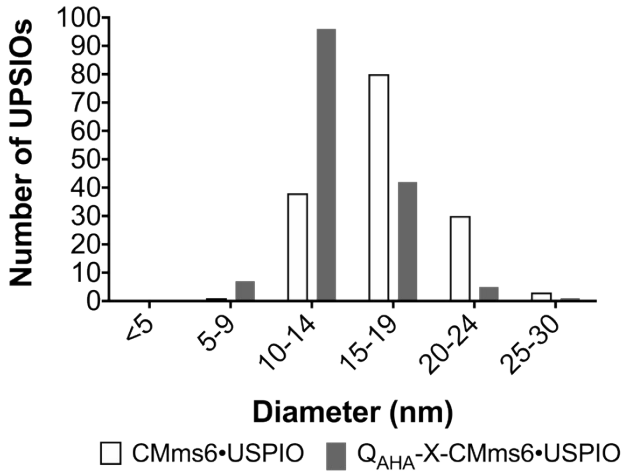

Figure S9. Size distribution of USPIOs visualized on brightfield TEM following co-precipitation reaction in the presence of CMms6 alone (CMms6•USPIO) or CMms6-conjugated Q_{AHA}-X-CMms6 (Q_{AHA}-X-CMms6•USPIO).

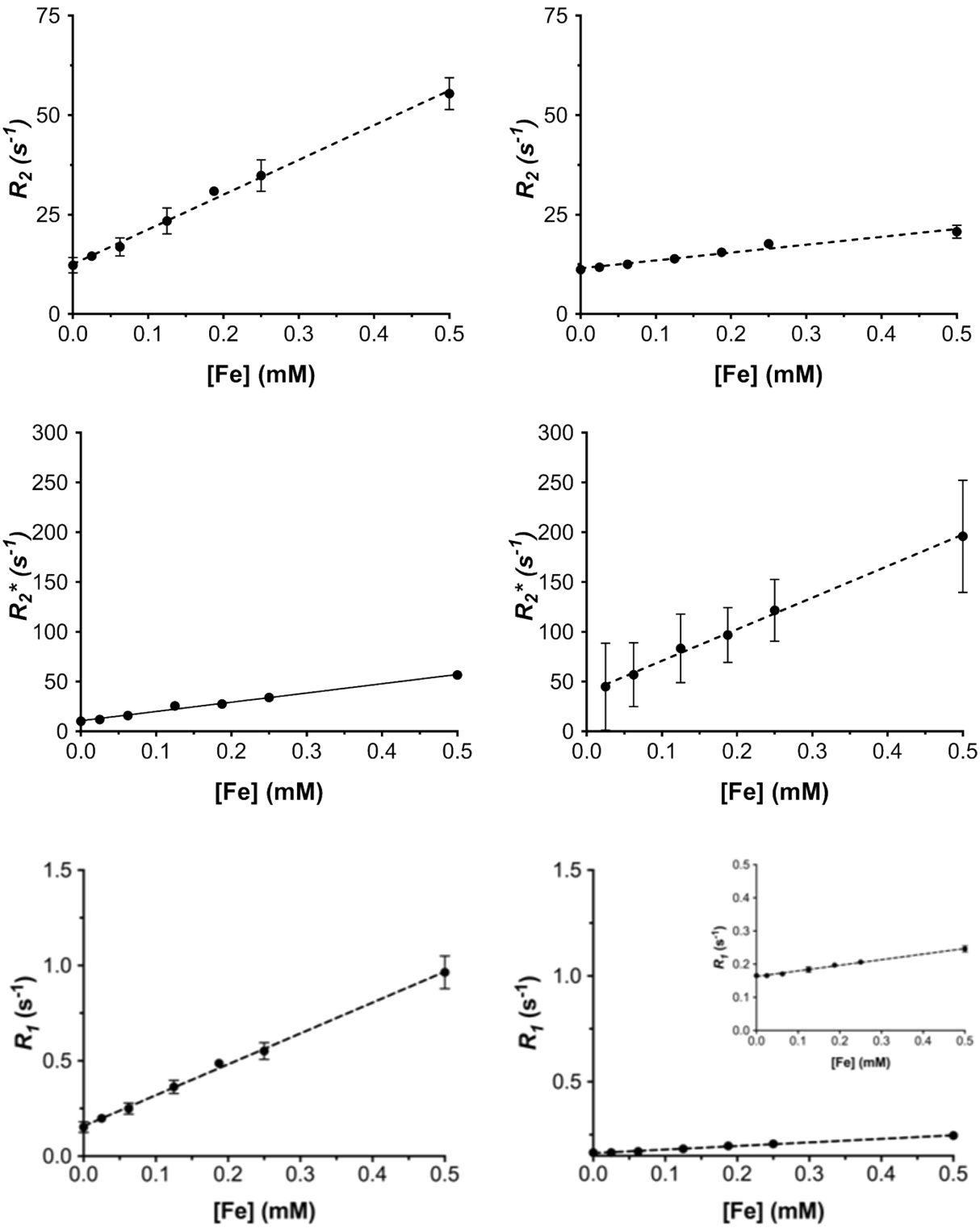
Feraheme
Q_{AHA}-X-CMms6•USPIO
R_2 (s^{-1})
R_2* (s^{-1})
R_1 (s^{-1})
[Fe] (mM)

Figure S10. Relaxation curves from magnetic resonance relaxometry. Relaxation rates, R_2, R_2* *and* R_1, as a function of iron concentration in Feraheme and Q_{AHA}-X-CMms6•USPIO. All data depict the average and standard deviation of three independent trials. Note the low R_1 relaxitvity of Q_{AHA}-X-CMms6•USPIO reflected by the weak slope in comparison to Feraheme. This was confirmed *in vivo* in tissue muscle

Table S1. Protein expression yield. Average Q_{WT} and Q_{AHA} yields from expression in M15MA *E.coli.* Data is reported as the mean value ± standard deviation.

Protein	Yield (mg L^{-1})
Q_{WT}	17.82 ± 4.44 (*N*=14)
Q_{AHA}	8.70 ± 1.58 (*N*=12)

Table S2. AHA Incorporation into the Q protein. Percent AHA incorporated into Q_{AHA} determined by MALDI-TOF MS and amino acid analysis. MALDI-TOF MS data is reported as the mean value ± standard deviation of six independent trails.

Method	AHA Incorporation (%)
MALDI-TOF MS	88.53 ± 5.03 (*N*=6)
Amino Acid Analysis *(UC Davis Genome Center)*	90.00

Table S3. Secondary structure of Q proteins in response to temperature. Mean residue ellipticity values from CD of Q_{WT} and Q_{AHA} at pH 4.0 from 25ºC to 85ºC and corresponding predicted secondary structure composition from CONTIN/LL assessment of the spectra. Data is reported as the average of three independent trials.

		Θ x 10^3 (deg·cm^2·dmol^{-1})			% composition		
		Θ_{222}	Θ_{min}	Θ_{222} / Θ_{min}	α-helix	β-content	unordered
25°C	Q_{WT}	-7.63	-16.28	0.47	56	21	23
	Q_{AHA}	-5.15	-14.25	0.36	55	24	21
35°C	Q_{WT}	-6.76	-16.54	0.41	67	33	-
	Q_{AHA}	-4.80	-13.95	0.34	55	26	20
45°C	Q_{WT}	-6.19	-16.13	0.38	55	17	27
	Q_{AHA}	-4.59	-13.77	0.33	51	49	-
55°C	Q_{WT}	-5.92	-15.93	0.37	69	31	-
	Q_{AHA}	-4.50	-13.43	0.33	49	39	12
65°C	Q_{WT}	-5.89	-15.68	0.38	51	28	21
	Q_{AHA}	-4.54	-13.29	0.34	52	34	14
75°C	Q_{WT}	-5.94	-15.43	0.38	46	18	36
	Q_{AHA}	-4.62	-12.86	0.36	50	25	25
85°C	Q_{WT}	-6.02	-15.24	0.39	54	34	13
	Q_{AHA}	-4.64	-12.51	0.37	48	19	32

Table S4. Mean residue ellipticity values from CD of Q proteins. Mean residue ellipticity values of Q_{WT} and Q_{AHA} pre and post-Dox binding and chemical crosslinking *via* BS^3. Data is reported as the average of three independent trials.

	$\Theta \times 10^3$ (deg·cm^2·dmol^{-1})		
	Θ_{222}	Θ_{min}	Θ_{222} / Θ_{min}
Q_{WT}	-7.63	-16.28	0.47
Q_{AHA}	-5.15	-14.25	0.36
Q_{WT}•Dox	-3.50	-8.97	0.39
Q_{AHA}•Dox	-2.64	-9.06	0.30
Q_{WT}•Dox_x	-11.80	-12.16	0.97
Q_{AHA}•Dox_x	-6.87	-8.44	0.81

Table S5. IC_{50} values of Dox and Q_{AHA}-X-CMms6•Dox treatment of MCF-7 cells *in vitro*. IC_{50} values calculated from CCK8 cell viability assays of MCF-7 cells treated *in vitro* with Dox and Q_{AHA}-X-CMms6•Dox for 24 hr and 48 hr. Data is reported as the mean value ± standard deviation of three independent trials.

Time	Treatment	IC_{50} (μM)
24 hr	Dox	2.92 ± 0.23 (*N* = 3)
	Q_{AHA}-X-CMms6•Dox	2.74 ± 0.31 (*N* = 3)
48 hr	Dox	1.28 ± 0.22 (*N* = 3)
	Q_{AHA}-X-CMms6•Dox	0.48 ± 0.11 (*N* = 3)

Table S6. Lattice *d*-spacing of USPIOs. Calculated lattice *d*-spacing from detectable small angle electron diffraction rings for USPIOs organized by Q_{AHA}-X-CMms6 (Q_{AHA}-X-CMms6•USPIO) compared to that reported for magnetite. Data is reported as the mean value ± standard deviation of three independent trials.

Ring	Q_{AHA}-CMms6•USPIO *d*-spacing (Å)	Magnetite (*Bragg et al*)[1]
1	1.150±0.00	1.18
2	1.33±0.00	1.32
3	1.37±0.00	1.37
4	1.52±0.00	1.51
5	1.65±0.00	1.64
6	1.74±0.00	1.74
7	2.12±0.01	2.11
8	2.55±0.00	2.54
9	2.95±0.02	2.97
10	4.80±0.04	4.82

1. Bragg, W.H., *The Structure of Magnetite and the Spinels.* Nature, 1915. **95**(2386): p. 561-561.